International Journal of Fluid Machinery and Systems
Vol. 2, No. 4, October-December 2009

Original Paper (Invited)

Overload Surge Investigation Using CFD Data

Felix Flemming[1], Jason Foust[1], Jiri Koutnik[2] and Richard K. Fisher[1]

[1]Voith Hydro, Inc.
760 East Berlin Rd., York, PA 17408, USA,
felix.flemming@voith.com, jason.foust@voith.com, richard.fisher@voith.com
[2]Voith Hydro Holding GmbH & Co. KG
Alexanderstr. 11, 89522 Heidenheim, Germany, jiri.koutnik@voith.com

Abstract

Pressure oscillations triggered by the unstable interaction of dynamic flow features of the hydraulic turbine with the hydraulic plant system - including the electrical design - can at times reach significant levels and could lead to damage of plant components or could reduce component lifetime significantly. Such a problem can arise for overload as well as for part load operation of the turbine. This paper discusses an approach to analyze the overload high pressure oscillation problem using computational fluid dynamic (CFD) modeling of the hydraulic machine combined with a network modeling technique of the hydraulic system. The key factor in this analysis is the determination of the overload vortex rope volume occurring within the turbine under the runner which is acting as an active element in the system. Two different modeling techniques to compute the flow field downstream of the runner will be presented in this paper. As a first approach, single phase flow simulations are used to evaluate the vortex rope volume before moving to more sophisticated modeling which incorporates two phase flow calculations employing cavitation modeling. The influence of these different modeling strategies on the simulated plant behavior will be discussed.

Keywords: Overload Surge, CFD, System Analysis, Cavitation, Vortex Rope, Francis Turbine

1. Introduction

During hydropower production, unstable flow characteristics within a Francis turbine draft tube may give rise to a phenomenon known as surge, whereby significant pressure oscillations in the cone can lead to the development of noise, vibrations, power swings, vertical displacement of the runner and shaft, as well as pressure disturbances that propagate back through the penstock [1][1]. Depending on the severity of the surge, these fluctuations can damage the mechanical and hydraulic system components within the unit.

Surge is related to swirl within the flow exiting the runner at off-design conditions. At part load operation, the circumferential velocity components are positive, creating a swirl that is co-rotational with the runner. Under conditions of overload, i.e., discharge rates greater than the flow associated with the best efficiency point, the swirl occurs in the opposite or counter-rotating direction [2], [3]. These developing swirl patterns (vortices) induce a region of low pressure near the center of the draft tube cone that can often drop below the liquid vapor pressure, causing air or water vapor to occupy the vortex core. The resulting vortices show distinct behavior relative to the flow rate at which they occur, leading to different surge characteristics. Photographs of the typical part load and overload cavitating vortices are given in Fig. 1.

The vortex associated with part load is helical in nature, rotating about the vertical axis of the machine [3], [4]. This recurring motion of the vortex causes a rotating velocity field within the draft tube cone, which then forces the periodic excitation leading to part load surge. At overload, the shape of the vortex changes to an elongated, torch-like structure shown in Fig. 1 (ii). Here the dynamics of the vortex rope can act as an energy source, leading to the development of self-excited oscillations and dynamic instabilities within the hydraulic system [3].

Accepted for publication May 27 2009: Paper number O09030S
Corresponding author: Felix Flemming, Manager CFD, felix.flemming@voith.com

This manuscript was presented at the 24th IAHR Symposium on Hydraulic Machinery and Systems, October 27-31, 2008, Foz do Iguassu-Brazil.

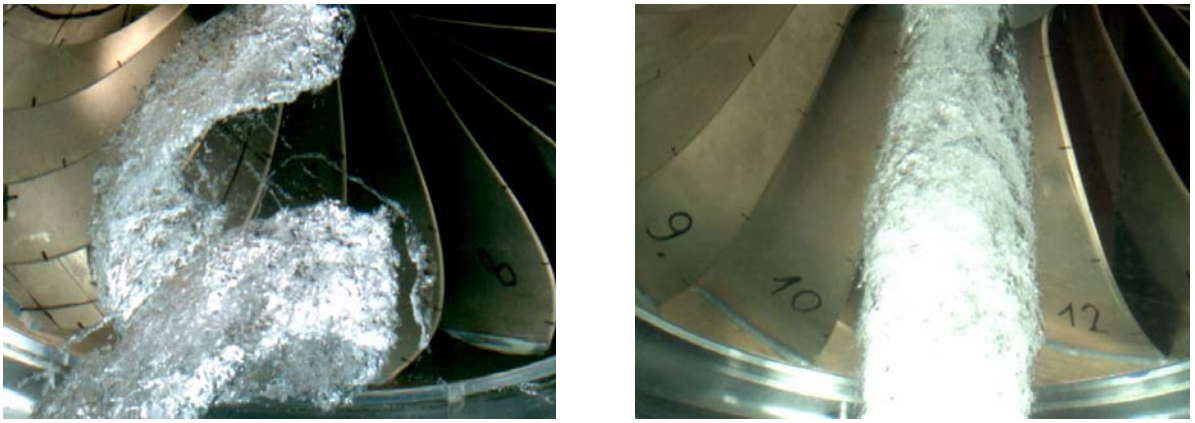

(i) (ii)

Fig. 1 Vortex rope for a Francis turbine at (i) part load and (ii) overload conditions.

In the past, prototype surge characteristics were derived from homologous model tests at hydraulically similar operating conditions. Under these circumstances, efficiency levels and cavitation information are quite reliable with the appropriate scaling and correction factors, but because discrepancies exist between the complete model and the prototype hydraulic circuit, this type of analysis has proven to be unreliable in regard to pressure pulsations [5]. Over the years, various mathematical models have been developed in order to gain further insight into surge characteristics, with the ultimate goal of being able to predict these instabilities during the design phase. One of the most well-known models bases the analysis on a 1D transfer matrix approach, where the elasticity of the vortex rope volume is one of the key parameters in the stability analysis [3], [6], [7], and [8]. While this analysis method has proven to be successful for select applications, determining the proper compliance factors induced by the prototype vortex rope characteristics remains challenging.

The current investigation explores the possibility of employing computational fluid dynamics (CFD) to determine the vortex rope characteristics for the case of overload surge in a typical Francis turbine with a specific speed of $Nq_{opt} = 60$, where

$$Nq_{opt} = \frac{N \cdot \left(Q_{opt} / 1\,m^3 s^{-1}\right)^{1/2}}{\left(H/1\,m\right)^{3/4}} \tag{1}$$

N represents the rotational speed of the runner, Q_{opt} is the flow rate at which the optimum efficiency occurs and H is the rated net head of the hydraulic plant.

In the description that follows, a detailed overview of the 1D dynamic system response analysis is provided, where the key parameters are identified, followed by a brief summary of the computational fluid dynamics setup, including the computational configuration and modeling used throughout the study. Finally, the CFD results are presented and used to draw conclusions about the overall feasibility of incorporating CFD analysis to accurately predict overload surge characteristics during turbine design.

2. System Analysis

Pressure pulsations at Francis turbine overload conditions are - contrary to the part load pressure oscillations - of a self-excited nature. The vapor filled vortex rope of a certain size, which is influenced by both the guide vane opening and the draft tube pressure, starts to interact with the stationary flow and the whole hydraulic system loses its dynamic stability and starts to oscillate.

In such a case, the system oscillates with one (or more) of its natural frequencies. The period of the oscillations (given by the imaginary part of the system complex natural frequency) is influenced above all by the so called vortex rope compliance, defined as a change of the vortex rope size with a change in draft tube pressure. For configurations with a longer penstock or tailwater system the influence of water compressibility may become significant as well.

The stability of the complete system is furthermore driven by another vortex rope parameter, which is often called mass flow gain factor (MFGF), defined by the change in vortex rope volume over the change in draft tube discharge. This MFGF may be understood as an energy source, which yields positive values in the overload operating range. This energy source transfers the energy from the steady flow into the oscillating behavior.

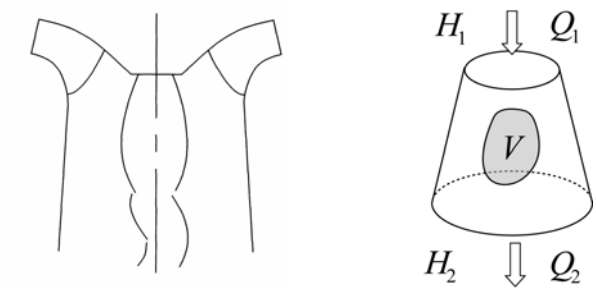

Fig. 2 Indices determination for overload surge.

The rate of change of the gaseous volume is given by the variation of discharge between the two fluid sections limiting the rope sketched in Fig. 2.

$$\frac{dV}{dt} = Q_2 - Q_1 \tag{2}$$

Here the vortex rope volume is basically a function of two state variables, i.e. discharge Q and draft tube pressure head H.

$$V(Q,H) \Rightarrow \frac{dV}{dt}\bigg|_2 = \frac{dV}{dH}\bigg|_2 \cdot \frac{dH_2}{dt} + \frac{dV}{dQ}\bigg|_2 \cdot \frac{dQ_2}{dt} \tag{3}$$

Using relation (3) equation (2) may be expressed as shown by (4).

$$Q_1 - Q_2 = C \cdot \frac{dH_2}{dt} + \chi \cdot \frac{dQ_2}{dt} \tag{4}$$

In the above expression (4) the two combined parameters are defined as:

- the cavity compliance $C = -\partial V / \partial H_2$ [m^2] (5)
- the mass flow gain factor (MFGF) $\chi = -\partial V / \partial Q_2$ [s] (6)

The system gets unstable when the energy supplied by the change in vortex rope volume exceeds the losses in the hydraulic system and the damping effect of the turbine, given by its Q-H characteristic, is insufficient.

A stability investigation of a general dynamic system can be efficiently carried out by using a modal analysis. This kind of analysis is performed to determine the stability domain of the hydraulic installation with respect to the combined parameters of the vortex rope, the rope compliance and mass flow gain factor respectively. For this purpose the transfer matrix method described in [6] is employed with advanced models of both friction losses and frequency dependent damping. The complex eigenvalues of the global system matrix are computed to derive both, the natural frequencies and the damping or amplification factors of the corresponding mode shape by means of the imaginary and real part of the eigenvalues respectively.

For example, the kth complex eigenvalue is expressed as $v_k = \alpha_k + i\omega_k$ where the real part α_k describes the mode shape damping and the imaginary part ω_k is the oscillation frequency in radians per second. The condition $\alpha_k > 0$ results in a dynamic unstable operation of the system, depicted by Fig. 3.

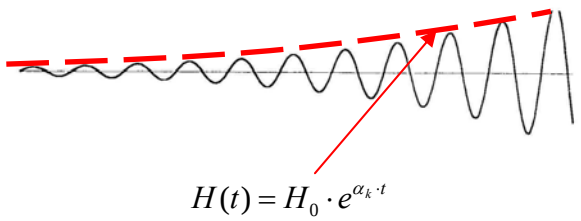

Fig. 3 System response to a disturbance under unstable conditions.

All identified potentially unstable combinations of vortex rope compliance and MFGF are then represented in a so called stability diagram, an example is given in Fig. 4, where all dots represent unstable vortex rope parameters for the hydraulic system in question. The MFGF scaling is represented on the left hand y-axis, while on the right hand y-axis the corresponding frequency of self-excited oscillations is shown. This frequency is a function of the vortex rope compliance and mass flow gain factor.

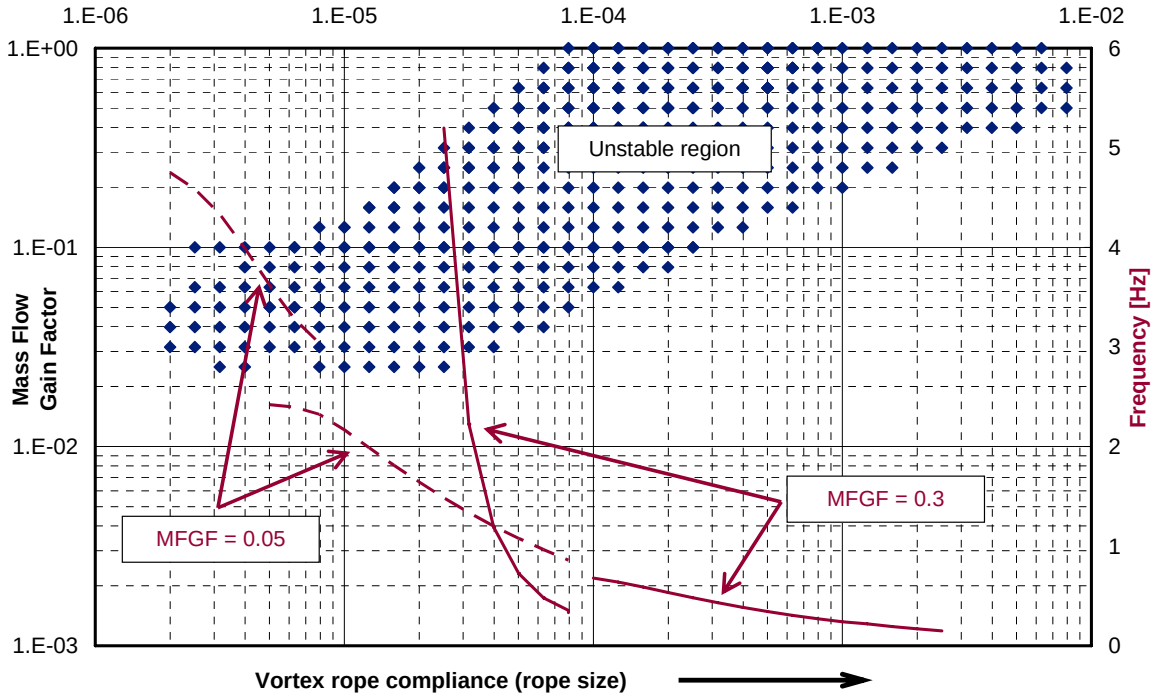

Fig. 4 Exemplary normalized stability diagram. The lines correspond to the unstable natural frequency of oscillation (y-axis on the right hand side) for the mass flow gain factor given in the accompanying box.

In order to perform the aforementioned stability analysis, accurate determination of the vortex rope volume and its rate of change with pressure and flow during conditions of overload is essential. Several procedures are possible for determining the volumes. Using a scaled model test one can estimate the vortex volume based on model observation. This methodology is based on the real physics but is subject to the individual person doing the observation and is also missing three dimensional input to some extent. Usually there would be an assumption on the rotational symmetry of the vortex rope such that a circular cross section can be utilized for the volume estimate. A second methodology is based on theoretical considerations. For such an approach numerous simplifying assumptions with respect to the physics need to be employed. A third methodology makes use of modern computer aided engineering (CAE) tools - computational fluid dynamics (CFD) and computer aided design (CAD) tools - and allows for an accurate vortex rope volume determination given that the underlying physics are captured in the numerical model of the fluid flow. This last approach will be highlighted and discussed in more detail in the remainder of this paper.

3. Configuration and Load Cases

Although the 1D dynamic system response analysis encompasses geometry from the turbine inlet through the draft tube exit, the determination of the vortex rope characteristics within the draft tube cone does not require such complete modeling. For the investigation herein, the computational domain consists of a single flow channel within the distributor section, i.e. flow between two sets of stay vanes and wicket gates, followed by the region located between two adjacent runner buckets. The final component of the model includes the full geometry of the draft tube. In an effort to minimize the computational time associated with each operating point while maintaining a high degree of accuracy, the simulations were conducted at model size. A complete representation of the computational domain is given in Fig. 5.

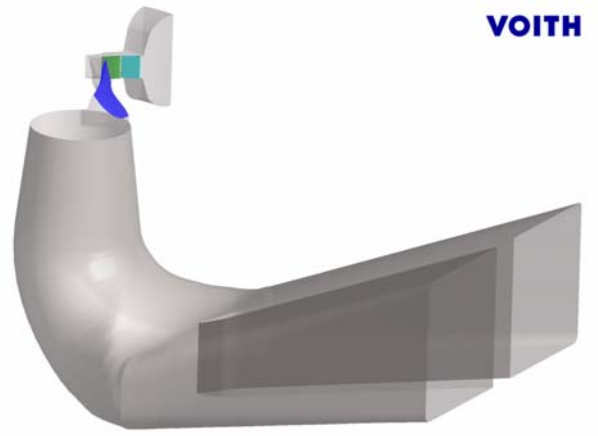

Fig. 5 Calculation geometry showing a view of the distributor, runner and draft tube.

When modeling the characteristics of the cavitating vortex associated within a scaled-down machine, additional care must be provided to ensure that the pressure gradient within the model draft tube matches that which occurs at prototype size. The appropriate pressure gradient within the model was achieved by adjusting the angular speed of the runner (ω) so that Froude similitude was maintained for the two different length scales. This dimensionless scaling parameter is expressed as

$$Fr = \frac{U^2}{gD} \tag{7}$$

where $U = (Q/A)$ is the average discharge velocity through the draft tube, g is the acceleration due to gravity and D is a characteristic length scale taken as the runner inlet diameter.

For the purpose of illustration, three operating conditions corresponding to overload will be discussed in relation to the cavitating vortex rope compliance and mass flow gain factors necessary for surge assessment. These operating conditions are given below in Table 1 in terms of normalized head H^*, flow rate Q^*, and Thoma number σ^*.

Table 1 Load case information.

Load Case	H^* [-]	Q^* [-]	σ^* [-]
LC01	0.97	1.22	0.88
LC02	0.97	1.22	1.00
LC03	1.05	1.28	0.88

Note that the Thoma number represents the cavitation index, given by the ratio of the net pressure suction head *NPSH* over the net head H

$$\sigma = \frac{NPSH}{H} = \frac{H_b - H_v - H_s}{H} \tag{8}$$

In equation (8), the variables H_b, H_v, and H_s correspond to the barometric head, the vapor head, and the suction head (reference elevation – tailwater elevation) for the operating condition under consideration.

LC01 and LC02 were selected to determine the cavitating vortex rope compliance factor C. These two conditions occur at the same net head and wicket gate opening, i.e. flow rate, but the different Thoma numbers signify a change in back-pressure (indicated as H_2 in Fig. 2). LC01 and LC03 differ in net head and flow rate under a constant back-pressure to enable the determination of the mass flow gain factor χ.

4. Computational Fluid Dynamics Setup

The numerical simulations were completed with the commercial ANSYS CFX 11.0 software package, which is widely accepted as a standard flow solver within the hydropower industry. With the appropriate model geometry established, an in-house automated block structured hexahedral meshing procedure was employed. For demonstrative purposes, the meshes resembling the various computational flow domains are shown in Fig. 6 for the LC01 example. The numerical mesh in total consists of approximately 2.4 Mio. grid nodes out of which 0.4 Mio. nodes correspond to the distributor section, 0.5 Mio. nodes represent the runner section and 1.5 Mio. nodes are utilized for the draft tube.

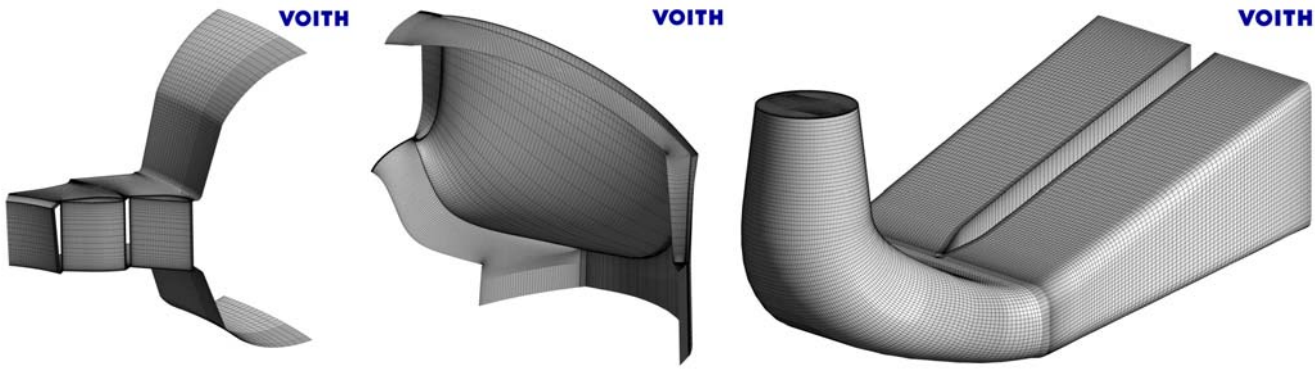

(i) (ii) (iii)

Fig. 6 Computational domains and meshes for (i) stay vane / wicket gate, (ii) runner, and (iii) draft tube.

For each operating condition, mass flow and flow direction relative to the inlet plane normal at the entrance to the distributor section were specified. At the outlet of the draft tube an averaged pressure boundary condition allowing for entrainment of flow has been utilized. In the case of the two phase flow simulations described below this outlet pressure had to be adjusted according to the scaled tailwater level for the load case considered. For the single phase simulations the pressure was simply set to 0 [Pa]. To all walls throughout the computational domain - stationary as well as rotating - a no slip boundary condition was applied. The interface between the stationary and rotating domains was modeled by stage interfaces which average the flow properties in circumferential direction. Such an interface is located between the tandem cascade and the runner as well as in between the runner and the draft tube.

To close the steady state Reynolds averaged transport equations the shear stress transport (SST) model has been employed for its well known accuracy in turbo machinery applications. In order to discretize the numerical fluxes, the high resolution advection scheme was chosen for spatial terms in accordance with the ANSYS CFX best practice guide lines [9]. In case of the two phase simulations performed in this study the cavitation model as provided and described by the ANSYS CFX modeling guidelines was used. Utilizing the correctly scaled outlet pressure the model allows to capture cavitation whenever the local pressure drops below the given saturation pressure of the water. This approach results in a water vapor volume fraction which then can be taken into account during the post processing of the results and the volume estimate for the vortex rope.

5. Results

For each of the two calculation approaches employed throughout the current investigation, visualization of the cavitating vortex rope volumes at each operating condition required the evaluation of separate parameters. The cavitating vortex rope volumes were determined by evaluating contours of constant Thoma number corresponding to the given tailwater settings for the single phase approach, while contours of constant water vapor volume fraction equal to 50% were utilized in case of the two phase calculations. These visualizations for the two different CFD modeling approaches are given in Fig. 7 (LC01), Fig. 8 (LC02), and Fig. 9 (LC03). Within each figure, the cavitating vortex volume (indicated by a red iso-surface) associated with the single phase approach is shown to the left, while the vortex core that corresponds to the two phase simulation is provided to the right. The contour in the back ground depicts to the normalized Thoma number distribution for the single phase CFD and the normalized absolute pressure distribution for the two phase simulations respectively.

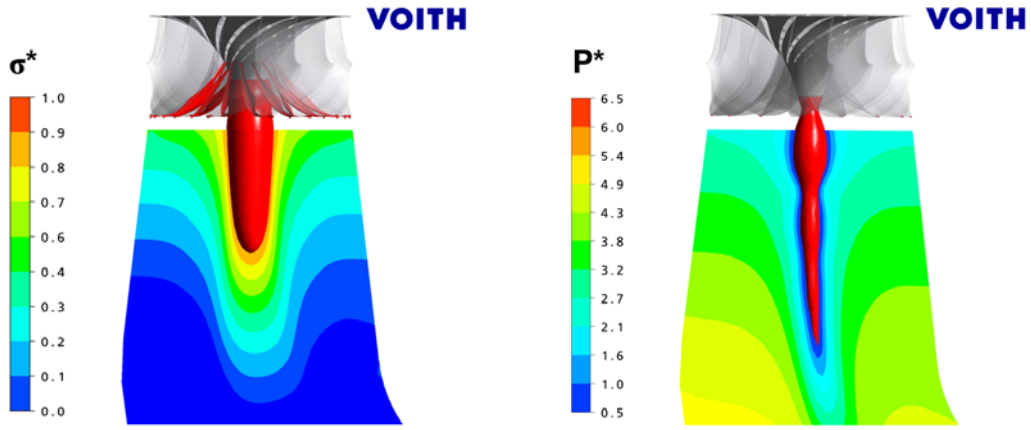

(i) (ii)

Fig. 7 Cavitating vortex rope volume using (i) single phase and (ii) two-phase flow calculations for load case LC01.

Starting with the first operating point (LC01) shown in Fig. 7, it is clear that while both calculation methodologies produce a cavitating vortex rope that resembles the torch-like structure as shown in Fig. 1 (ii), significant differences exist between the two procedures in regard to size, shape, and location. The cavitating vortex rope that occurs in the left image (single phase) consists of a much larger cross-section and attaches closer to the runner blades on the hub when compared to the results of the two phase calculation given to the right. At this operating condition, the length of the vortical structure predicted by the single phase approach extends only half the distance covered by the second, two phase approach. The additional complexity of the two phase approach is apparent when cross-comparing the surface contours associated with the different simulations. Surface irregularities result from the two phase calculation, while the iso-surface of constant Thoma number is very uniform in regard to both the radial and streamwise direction. This increased level of detail provided by the two phase approach as well as the longer volume extending into the draft tube elbow is consistent with model observations performed at similar operating conditions.

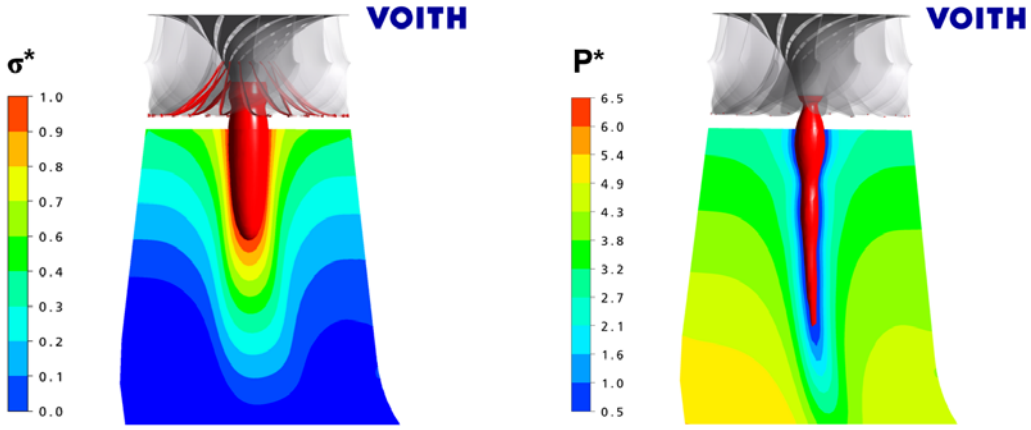

(i) (ii)

Fig. 8 Cavitating vortex rope volume using (i) single phase and (ii) two-phase flow calculations for load case LC02.

Vortex rope volumes corresponding to LC02 are given in Fig. 8. The features of the cavitating vortex rope visualizations are very consistent with those observed in Fig. 7 for the lower Thoma number and therefore lower back pressure. The single phase approach provides a smooth surface contour that exhibits a relatively uniform thickness throughout the draft tube cone, while the two phase results show a more detailed structure. For this operating point, the cavitating vortex rope volumes are smaller than those observed in Fig. 7, corresponding to the increase in back-pressure at the draft tube exit location. This behavior of the numerical model is in line with model test observations varying the tailwater level of the model setup.

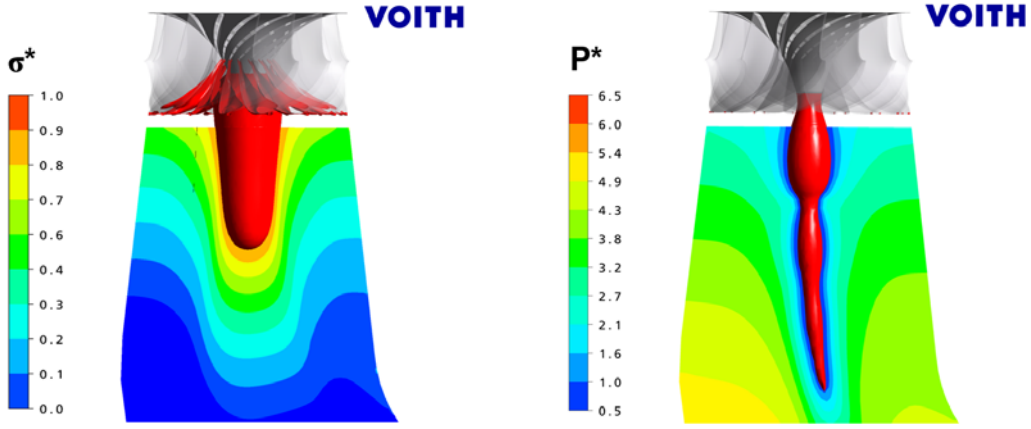

(i) (ii)

Fig. 9 Cavitating vortex rope volume using (i) single phase and (ii) two-phase flow calculations for load case LC03.

The results for the final operating point, load case LC03, are given in Fig. 9. For both the single and two phase calculations, the increase in flow rate has lead to a significant increase in the predicted cavitation region downstream of the runner. Again, this aligns with observations on model turbines in the laboratory. As with the previous load cases shown in Fig. 7 and Fig. 8, the surface contour associated with the single phase approach is much more uniform than that which occurs for the two phase calculation. Both modeling strategies result in the correct behavior with respect to changing boundary conditions, e.g. tailwater level or flow rate of the model. Nevertheless, the single phase flow does not capture the shape or the attachment point of the cavitating vortex rope volume correctly.

In order to determine the cavitating vortex rope volumes for each load case and calculation method, point clouds defining the iso-surface of constant Thoma number and water vapor volume fraction where exported from ANYSIS CFX and imported into the Unigraphics (UGS) NX5 computer aided design (CAD) software package. Once in the CAD system, the point cloud was converted into a solid body for which the determination of geometric properties such as volume is a standard function. A further advantage of the CAD system is its ability to easily compare the volumes directly. Such a comparison is given in Fig. 10 for LC01. Here, the different attachment point and size of the vortex volume for the two modeling approaches - single phase vs. two phase - can be seen clearly. In addition to being efficient, the use of CAD to determine the cavitating vortex rope volumes provides a standardized calculation procedure that minimizes variations and errors resulting from user estimation. Moreover, asymmetries of the vortex rope are easily accounted for when determining its volume. The vortex rope volumes calculated in the CAD system are given below in Table 2. Obviously, any other tool to calculate the vortex rope volumes can be used to retrieve the identical information. Note that the volume values are scaled back to the corresponding prototype size in order to be applicable in the system analysis described before.

Fig. 10 Comparison of single phase (blue) vs. two phase (red) vortex volume for LC01 in CAD.

Table 2 Prototype vortex rope volumes, compliances, and mass flow gain factors for the two CFD modeling approaches.

Load Case	Single Phase CFD			Two Phase CFD		
	Volume [m^3]	Compliance* [-]	MFGF* [-]	Volume [m^3]	Compliance* [-]	MFGF* [-]
LC01	8.6	7.05e-05	0.120	3.3	2.16e-05	0.105
LC02	5.9			2.7		
LC03	14.4			6.4		

For each of the load cases under investigation, the vortex rope volumes resulting from the two phase calculations are a factor of approximately 2 to 3 times smaller than those determined from the single phase calculations. The volumes given in Table 2 were then used to determine the cavitation compliance factor C, and mass flow gain factor χ, for each calculation procedure. The normalized results are shown in the adjacent columns. Although the single and two phase flow calculations lead to different stability parameters, both sets of values resulted in the prediction of unstable prototype operation. This can easily be seen when comparing the CFD results with the initial stability diagram discussed before (see Fig. 11).

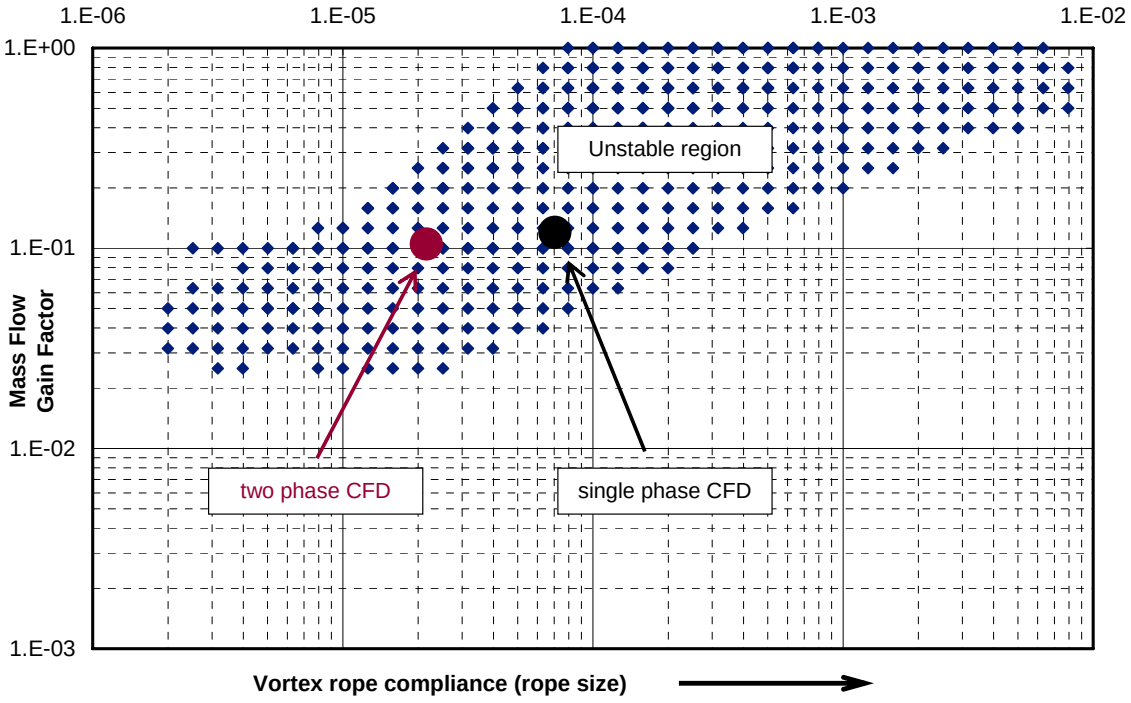

Fig. 11 Normalized stability diagram showing the two different CFD based evaluations.

6. Conclusions

The current investigation has studied the feasibility of implementing computational fluid dynamic (CFD) calculations to determine cavitating vortex rope characteristics and stability parameters (cavitation compliance factors C, and mass flow gain factor χ) under overload conditions. Two different numerical approaches were employed, including a single phase method in addition to a two phase, cavitation model. Each calculation procedure produced results that lead to predictions consistent with prototype and model observations, indicating that CFD is a viable tool for evaluating conditions leading to overload surge. Although the end result of the stability analysis procedure was similar for both calculation methodologies for the investigated system, the individual vortex rope volumes, i.e. the compliance and mass flow gain factors, were significantly influenced by the calculation methodology (see Table 2). However, this new approach helped to better understand the full-load surge phenomena described in [3] by quantitative comparison of calculated oscillation frequency and onset of the instability. The comparison of the simulated cavitating vortex cores with model observations made at similar operating conditions reveals that the two phase calculation provides surface contours that agree qualitatively very well, while the single phase approach deviates strongly. It can therefore be concluded that despite both calculation procedures providing the similar outcomes for the operating points included in the current investigation, analysis of other operating points closer to the stability threshold will be influenced by the different cavitation characteristics resulting from the one and two phase methodologies.

It has been demonstrated that computational fluid dynamics simulations can be utilized in conjunction with existing 1D stability analysis procedures to reasonably predict overload surge. Although the two phase approach involves slightly longer computational times, the simulated results have correlated better with physical observations and are expected to result in a more accurate inception prediction. The procedure outlined herein for calculating overload surge characteristics and the resulting stability analysis is a valuable tool for turbine design that can be implemented on a regular basis. Other areas of application include the investigation of part load surge resulting from forced oscillations induced by the helical vortex rope. Here, unsteady two phase simulations are required to capture the non-symmetric behavior of the vortex rope. For both part load and overload flow regimes, computational fluid dynamics can be utilized to provided detailed insight in surge characteristics already in the design phase of a turbine. This allows the appropriate measures to be taken early in the project to avoid large problems and therefore cost in the field after the erection of the equipment.

Nomenclature

A	Cross sectional surface [m^2]	α_k	Real part of complex eigenvalue (mode shape damping [1/s])
C	Cavity compliance [m^2]	σ	Thoma number [-]
D	Characteristic length scale [m]	χ	Mass flow gain factor (MFGF) [s]
Fr	Froude number [-]	ω	Angular speed [1/s]
g	Acceleration due to gravity [m/s^2]	ω_k	Imaginary part of complex eigenvalue (oscillation frequency [1/s])
H	Rated net head [m]		
H_1, H_2	Head [m]		
H_b	Barometric head [m]		
H_v	Vapor head [m]	$\cdot^*$	Normalized quantity
H_s	Suction head [m]		
$NPSH$	Net pressure suction head [m]	$\cdot_0$	Value at $t = 0$ [s]
Nq	Specific speed [rpm]	$\cdot_1$	Position at inlet to draft tube cone
N	Rotational speed [rpm]	$\cdot_2$	Position at outlet of draft tube cone
P	Absolute pressure [Pa]	$\cdot_b$	Barometric value
Q_{opt}, Q_1, Q_2	Flow rate [m^3/s]	$\cdot_k$	k^{th} eigenmode
t	Time [s]	$\cdot_{opt}$	Quantity for optimum operating condition
U	Average discharge velocity ($=Q/A$) [m/s]	$\cdot_s$	Suction value
v_k	Eigenvalue of global system matrix [1/s]	$\cdot_v$	Vapor value
V	Vortex rope volume [m^3]		

References

[1] Falvey, H., 1971, “Draft tube surges. A review of the present knowledge and annotated bibliography”, Bureau of Reclamation Report REC-ERC-71-42, Denver, Colorado, USA.

[2] Aschenbrenner, T., Otto, A., Moser, W., 2006, “Classification of vortex and cavitation phenomena and assessment of CFD prediction capabilities”, 23rd IAHR Symposium, Yokohama, Japan.

[3] Koutnik, J., Nicolet, C., Schohl, G., Avellan, F., 2006, “Overload surge event in a pumped-storage power plant”, 23rd IAHR Symposium, Yokohama, Japan.

[4] Jacob, T., Prenat, J., 1996, “Francis turbine surge: discussion and data base”, 18th IAHR Symposium, Valencia, Spain.

[5] Doerfler, P., 1982, “System dynamics of the Francis turbine half load surge”, 11th IAHR Symposium, Amsterdam, Netherlands.

[6] Koutnik, J., 2000, “Analysis of pressure oscillations measured in the twin-penstock of PSPP Stechovice”, 20th IAHR Symposium, Charlotte, North Carolina, USA.

[7] Philibert, R., Couston, M., 1998, “Francis turbines at part load: matrix simulating the gaseous rope”, 19th IAHR Symposium, Singapore.

[8] Brennan, J., Acosta, A., 1973, “Theoretical quasi-static analysis of cavitation compliance in turbopumps”, Journal of Spacecraft and Rockets, Vol. 10, No. 3, pp. 175--180.

[9] ANSYS CFX Release 11.0, “ANSYS CFX-Solver Modeling Guide”, ANSYS Europe, Ltd. 1996-2006.